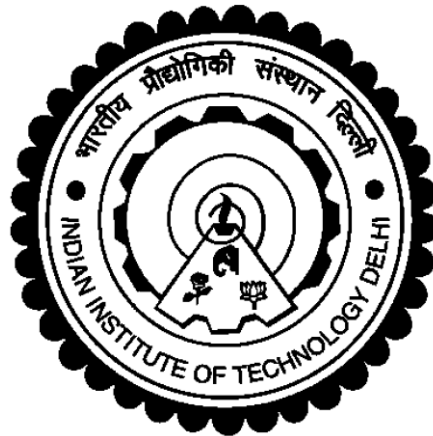


DESIGN AND CONTROL OF HIGH POWER GRID INTERFACED SOLAR PV SYSTEM WITH BES

SUBIR KARMAKAR



**DEPARTMENT OF ELECTRICAL ENGINEERING
INDIAN INSTITUTE OF TECHNOLOGY DELHI
HAUZ KHAS, NEW DELHI-110016, INDIA
DECEMBER 2022**

© Indian Institute of Technology Delhi (IITD), New Delhi-110016

**DESIGN AND CONTROL OF HIGH POWER GRID
INTERFACED SOLAR PV SYSTEM WITH BES**

by

SUBIR KARMAKAR
Electrical Engineering Department

Submitted

in fulfillment of the requirements of the degree of Doctor of Philosophy

to the



INDIAN INSTITUTE OF TECHNOLOGY DELHI
DECEMBER 2022

CERTIFICATE

It is certified that the thesis entitled “**Design and Control of High Power Grid Interfaced Solar PV System With BES,**” being submitted by **Mr. Subir Karmakar** for award of the degree of **Doctor of Philosophy** in the Department of Electrical Engineering, Indian Institute of Technology Delhi, is a record of the student work carried out by him under my supervision and guidance. The matter embodied in this thesis has not been submitted for award of any other degree or diploma.

Dated: December 26, 2022

(Prof. Bhim Singh)
Electrical Engineering Department
Indian Institute of Technology Delhi
Hauz Khas, New Delhi-110016, India

ACKNOWLEDGEMENTS

I wish to express my deepest gratitude and indebtedness to **Prof. Bhim Singh** for providing me guidance and constant supervision to carry out the Ph.D. work. Working under him has been a wonderful experience, which has provided a deep insight to the world of research. Determination, dedication, innovativeness, resourcefulness and discipline of **Prof. Bhim Singh** have been the inspiration for me to complete this work. His consistent encouragement, continuous monitoring and commitments to excellence have always motivated me to improve my work and use the best of my capabilities. Due to his blessing, I have earned various experiences, other than research, which will help me throughout my life.

My sincere thanks and deep gratitude are to **Prof. Sukumar Mishra, Prof. G. Bhuvanewari, and Prof. Ashu Verma**, all SRC members for their valuable guidance and consistent support during my research work.

I wish to convey my sincere thanks to **Prof. Bhim Singh, Prof. M. L. Kothari, Prof. T. S. Bhatti, late Prof. K. R. Rajagopal, Prof. Sukumar Mishra, and Prof. G. Bhuvanewari** for their valuable inputs during my course work, which made the foundation for my research work. I am grateful to IIT Delhi for providing me the research facilities. I would wish to express my sincere gratitude to **Prof. Bhim Singh, Prof. G. Bhuvanewari, late Prof. K. R. Rajagopal, and Prof. M. Veerachary** as Prof. in-charge of PG Machine Lab, for providing me immense facilities to carry out experimental work. Thanks are due to Mr. Srichand, Mr. Puran Singh, and Mr. Jitendra and Mr. Anurag, of PG Machines Lab., IIT Delhi for providing me the facilities and assistance during this work.

I would like to thank all my seniors, Dr. Shailendra Sharma, Dr. Ashish Shrivastava, Dr. Sandeep V., Dr. Ram Niwas, Dr S.K. Tiwari, to motivate me in the starting of my research work.

I would like to use this opportunity to thank Dr. N. K. Swami Naidu, Dr. Nidhi Mishra, Mr. Anshul Varshney, Mr. Shivam Kumar Yadav, Dr. Sabharaj Arya, Dr. M. Sandeep, Dr. Vashist Bist, Dr. Ikhtlaq Hussain, Dr. Anjaneer Kumar Mishra, and Mr. Aryadip Sen who have constantly helped me on all technical and non technical issues. I also wish to take this opportunity to thank Mr. Utkarsh Sharma, Ms. Rashmi Rai, Mrs. Yashi Singh, Mr. Vineet P Chandra, Mr. Priyank Shah, Mr. Dipu Vijaya M, Mrs. Shataskshi Sharma, Mrs. Aakanksha Rajput, Mr. Vivek Narayanan, Mr. Debasish Mishra, Mr. Anjeet Verma, Mr. Gurmeet Singh, Mr. Sreejith R, Dr. Radha Kushwaha, Mrs. Vandana Jain, Ms. Seema Kewat, Mrs. Subhra, Mrs. Farheen Chishti, Mrs. Pavitra Shukl, Ms. Sunaina Singh, Mr. Sai Pranith Girimaji, Mr. Tripurari Nath, Mr. Gaurav Modi, Mr. Bilal Naqvi, Mr. K.P. Tomar, Mr. Sunil Pandey, Ms. Shalvi Tyagi, Mrs. Rohini Sharma, Ms. Chandrakala, Ms. Kousalya, Mr. Kashif, Mr. Sharan Shastri, Ms. Hina Parveen, Mr. Yalavarthi Amarnath, Mr. VL Srinivas, Mr. Priyabrat Vats, Mr. Suri Paneeth, Mr. Jitendra Gupta, Mr. Rahul Kumar, Mr. Sayandev Ghosh, Mr. Utsav Sharma, Mr. Saran Chourasiya, Mr. Shivam Yadav, Mr. Deepak shaw, Mr. Sambasivaiah, Mr. Sudip Bhattacharya, Mr. Sandeep Sahoo, Mr. Souvik Das, Ms. Kripa, Ms. Farha Siddique, Mr. Zarkab, Mr. Saurabh, Mr. Vipin, Mr. Rohit, Mr. Arjun, Mr. Biswajit, Mr. Sumit, Mr. Himanshu, Mr. Girja Shankar and all PG Machines lab group for their valuable support. I would also like to thank Mr. Satish, Mr. Yatindra, Mr. Narendra, Mr. Sandeep, Ms. Moni and all other electrical engineering office staff for being supportive throughout. I am likewise thankful to those who have directly or indirectly helped me to finish my dissertation study.

I would like to thank my Mother, Mrs. Usharani Karmakar, Father, Mr. Hemanta Karmakar, Brother, Uttam Karmakar for their dreams, blessings, and constant encouragement. I would like to thank my Wife, Mrs. Sanchita Mitra and my Son Mr. Adrik Karmakar for giving me the inner strength and wholehearted support. I would like to thank my younger sisters, Mrs. Sima

Karmakar and Mrs Aparna Karmakar, and all my family members for their continuous support and encouragement. Their trust in my capabilities had been a key factor to all my achievements.

At last, I am beholden to almighty for their blessings to help me to raise my academic level to this stage. I pray for their benediction in my future endeavours. Their blessings may be showered on me for strength, wisdom and determination to achieve in future.

Dated: December 26, 2022

Subir Karmakar

ABSTRACT

In this thesis work, high-power grid interfaced solar PV plants and battery energy storage (BES) systems utilizing fundamental frequency switching (FFS) modulated different multipulse and multilevel voltage source converters (VSCs) topologies are investigated in detail. Investigations are made on 52MWp grid interfaced solar PV plant based on multipulse VSCs utilizing FFS modulated two-level converters with different switching phase displacement angles and star-delta medium voltage (MV) transformers. The transformers primary sides (HV side) are series connected to electro-magnetically add the converters generate voltage for direct integration to the 33kV grid. The investigations are also made on a 100MWp grid interfaced solar PV plant based on 48-pulse VSCs utilizing star-delta MV transformer and FFS modulated three-level neutral point clamp converters (NPCs). Two different MV transformer configurations are used, one with delta-star and another with delta-delta transformer configurations. The transformer secondary delta open windings are separated phase-by-phase, and the primary star and delta windings are series-connected. In this multipulse VSC configuration, the harmonics mitigation is achieved by operating the NPCs with different switching phase displacement angles and fixed voltage dead-angle. The VSC dead-angle is optimally selected, and VSC works as equivalent to a 96-pulse VSC for harmonics mitigation. The VSC output voltage amplitude control is realized with two sets of NPCs operated with leading and lagging voltage angles to provide lagging, leading, and unity power factor operation. Grid interfaced 40MWp solar PV plant configured with FFS modulated three-level-NPC and different phase-shifted 12-pulse transformers is investigated in detail. In this, the FFS modulated NPCs generated lower order current harmonics and are mitigated by utilizing different phase-shifting transformer windings located at different pooling

locations inside the solar plant. The plant generates low current harmonics similar to a 48-pulse converter at the 33kV grid connection.

Investigations are made on grid interfaced solar PV plant of capacity 240MWp with DC coupled BES of 120MW/720MWh configured with high-power 72-pulse VSC. The 72-pulse VSC is configured with NPCs with suitably selected switching angles and MV transformer with different phase-shifted zigzag secondary windings and series-connected star primary winding. The NPCs are divided into two groups, Group-A NPCs are connected with the line side of zigzag windings, and Group-B NPCs are connected with the neutral side of the zigzag windings. The NPCs dead angle (β) is controlled to control the VSC output voltage amplitude. The multi-MPPT technique is applied to this single-stage VSC for optimal solar power generation. In the large solar PV plant area, the BES is deployed along with the solar PV array and locally stores the excess solar PV energy and dispatches the stored energy during nighttime when the solar PV array is not generating. A 225MWp solar PV plant based on 54-pulse VSCs is also investigated. The 54-pulse VSC is developed with identical three sets of 18-pulse VSCs, each configured with two-level converters (TLCs) and a step-up transformer with series-connected star and different phase-shifted zigzag primary windings, and delta-connected secondary windings. The 54-pulse VSC operation is realized with suitably selected TLCs switching phase displacement angles and 18-pulse VSC transformer configuration. A 112.5MW/450MWh BES is DC coupled at the VSCs DC terminals for storing surplus solar energy and supply to the grid during non-solar hours. Investigations are also made on grid interfaced 480MWp solar PV plant based on 96-pulse modular VSC. Four sets of modular 24-pulse VSC having identical power circuit configurations are utilized to develop the 96-pulse VSC. Each 24-pulse VSC is configured with three-level converters and transformers with delta open LV-windings and series connected different phase-shifted zigzag HV-windings. The

solar PV plant is integrated to the 66kV grid. The 96-pulse VSC lower order harmonic elimination is realized with the multipulse transformer (MPT) configuration, and higher order harmonics are eliminated with the suitably selected converters switching angles based on selective harmonics elimination (SHE) techniques. The MPPT DC-DC boost converter is used with each PV string for optimum solar generation. A battery energy storage system (BES) is connected in the field with the PV sub-array to provide the grid Round-the-Clock Power (RTC) supply.

Investigations are made on high-power grid interfaced solar PV plants based on multilevel converters (MLCs). Fundamental frequency switching selective harmonic elimination (SHE) modulated eleven-level cascaded H-bridge (CHB) VSC is utilized in MLC applications. The eleven-level CHB VSC configuration and control algorithms with the capacitor voltage balancing method are presented in detail. Investigations are also made on BES based on 13-level CHB VSC utilized to mitigate 20MW solar PV plant power fluctuation and energy time shifting/peak shifting applications. A hybrid smoothing method is presented, suitable for sunny and cloudy weather conditions and optimizing the battery energy uses and sizing. The battery state of charge (SOC) control and VSC area equalization modulation strategy (AEMS) is presented in detail.

The design, modelling, control, and real-time implementation of the various plant configurations of high power grid interface solar PV, and BES systems as discussed above have been carried out, and their steady-state, harmonic, and dynamic performances, STATCOM operation, are evaluated under varying solar irradiance levels and change in grid voltages.

सारांश

इस थीसिस कार्य में, हाई-पावर ग्रिड इंटरफेसड सोलर पीवी प्लांट्स और बैटरी एनर्जी स्टोरेज (बीईएस) सिस्टम, जो मौलिक फ्रीक्वेंसी स्विचिंग (एफएफएस) मॉड्युलेटेड विभिन्न मल्टीपल्स और मल्टीलेवल वोल्टेज सोर्स कन्वर्टर्स (वीएससी) टोपोलॉजी का उपयोग करते हैं, की विस्तार से जांच की जाती है। विभिन्न स्विचिंग चरण विस्थापन कोणों और स्टार-डेल्टा मध्यम वोल्टेज (एमवी) ट्रांसफॉर्मर के साथ एफएफएस मॉड्युलेटेड दो-स्तरीय कन्वर्टर्स का उपयोग करते हुए मल्टीपल्स वीएससी पर आधारित 52MW_p ग्रिड इंटरफेसड सोलर पीवी प्लांट पर जांच की जाती है। ट्रांसफॉर्मर प्राथमिक पक्ष (एचवी पक्ष) विद्युत-चुंबकीय रूप से जुड़े श्रृंखला हैं जो कन्वर्टर्स को 33kV ग्रिड के प्रत्यक्ष एकीकरण के लिए वोल्टेज उत्पन्न करते हैं। स्टार-डेल्टा एमवी ट्रांसफॉर्मर और एफएफएस मॉड्युलेटेड थ्री-लेवल न्यूट्रल पॉइंट क्लैम्प कन्वर्टर्स (एनपीसी) का उपयोग करने वाले 48-पल्स वीएससी पर आधारित 100MW_p ग्रिड इंटरफेसड सोलर पीवी प्लांट पर भी जांच की जाती है। दो अलग-अलग एमवी ट्रांसफॉर्मर कॉन्फिगरेशन का उपयोग किया जाता है, एक डेल्टा-स्टार के साथ और दूसरा डेल्टा-डेल्टा ट्रांसफॉर्मर कॉन्फिगरेशन के साथ। ट्रांसफॉर्मर सेकेंडरी डेल्टा ओपन वाइंडिंग्स को चरण-दर-चरण अलग किया जाता है, और प्राथमिक स्टार और डेल्टा वाइंडिंग्स श्रृंखला से जुड़े होते हैं। इस मल्टीपल्स वीएससी कॉन्फिगरेशन में, एनपीसी को विभिन्न स्विचिंग चरण विस्थापन कोणों और फिक्स्ड वोल्टेज डेड-एंगल के साथ संचालित करके हार्मोनिक्स शमन प्राप्त किया जाता है। वीएससी डेड-एंगल इष्टतम रूप से चुना गया है, और वीएससी हार्मोनिक्स शमन के लिए 96-पल्स वीएससी के बराबर काम करता है। वीएससी आउटपुट वोल्टेज आयाम नियंत्रण को लैगिंग, लीडिंग और यूनिटी पावर फैक्टर ऑपरेशन प्रदान करने के लिए अग्रणी और लैगिंग वोल्टेज कोणों के साथ संचालित एनपीसी के दो सेटों के साथ महसूस किया जाता है। एफएफएस मॉड्युलेटेड थ्री-लेवल-एनपीसी और अलग-अलग फेज-शिफ्ट किए गए 12-पल्स ट्रांसफॉर्मर के साथ कॉन्फिगर किए गए ग्रिड इंटरफेसड 40MW_p सोलर पीवी प्लांट की विस्तार से जांच की

गई है। इसमें, एफएफएस मॉड्यूलैटेड एनपीसी ने लोअर ऑर्डर करंट हार्मोनिक्स उत्पन्न किया और सोलर प्लांट के अंदर विभिन्न पूलिंग स्थानों पर स्थित विभिन्न फेज-शिफ्टिंग ट्रांसफॉर्मर वाइंडिंग का उपयोग करके इसे कम किया गया। संयंत्र 33kV ग्रिड कनेक्शन पर 48-पल्स कनवर्टर के समान कम वर्तमान हार्मोनिक्स उत्पन्न करता है।

उच्च शक्ति 72-पल्स वीएससी के साथ कॉन्फ़िगर किए गए 120MW/720MWh के डीसी युग्मित बीईएस के साथ 240MWp क्षमता के ग्रिड इंटरफ़ेस वाले सौर पीवी संयंत्र पर जांच की जाती है। 72-पल्स वीएससी को एनपीसी के साथ उपयुक्त रूप से चयनित स्विचिंग एंगल्स और एमवी ट्रांसफॉर्मर के साथ अलग-अलग फेज-शिफ्ट किए गए ज़िगज़ैग सेकेंडरी वाइंडिंग और सीरीज़-कनेक्टेड स्टार प्राइमरी वाइंडिंग के साथ कॉन्फ़िगर किया गया है। एनपीसी को दो समूहों में बांटा गया है, ग्रुप-ए एनपीसी ज़िगज़ैग वाइंडिंग के लाइन साइड से जुड़े हैं, और ग्रुप-बी एनपीसी ज़िगज़ैग वाइंडिंग के तटस्थ पक्ष से जुड़े हैं। वीएससी आउटपुट वोल्टेज आयाम को नियंत्रित करने के लिए एनपीसी डेड एंगल (β) को नियंत्रित किया जाता है। इष्टतम सौर ऊर्जा उत्पादन के लिए मल्टी-एमपीपीटी तकनीक इस सिंगल-स्टेज वीएससी पर लागू होती है। बड़े सौर पीवी संयंत्र क्षेत्र में, बीईएस सौर पीवी सरणी के साथ तैनात किया जाता है और अतिरिक्त सौर पीवी ऊर्जा को स्थानीय रूप से संग्रहीत करता है और सौर पीवी सरणी उत्पन्न नहीं होने पर रात के समय संग्रहीत ऊर्जा को भेजता है। 54-पल्स वीएससी पर आधारित 225MWp सोलर पीवी प्लांट की भी जांच की जा रही है। 54-पल्स वीएससी को 18-पल्स वीएससी के समान तीन सेटों के साथ विकसित किया गया है, प्रत्येक को दो-स्तरीय कन्वर्टर (टीएलसी) के साथ कॉन्फ़िगर किया गया है और श्रृंखला से जुड़े स्टार और विभिन्न चरण-स्थानांतरित ज़िगज़ैग प्राथमिक वाइंडिंग्स और डेल्टा- के साथ एक स्टेप-अप ट्रांसफॉर्मर है। कनेक्टेड सेकेंडरी वाइंडिंग। 54-पल्स वीएससी ऑपरेशन उपयुक्त रूप से चयनित टीएलसी स्विचिंग चरण विस्थापन कोण और 18-पल्स वीएससी ट्रांसफॉर्मर कॉन्फ़िगरेशन के साथ महसूस किया जाता है। 112.5MW/450MWh बीईएस, वीएससी

डीसी टर्मिनलों पर अधिशेष सौर ऊर्जा के भंडारण और गैर-सौर घंटों के दौरान ग्रिड को आपूर्ति करने के लिए डीसी युग्मित है। 96-पल्स मॉड्यूलर VSC पर आधारित ग्रिड इंटरफेस 480MWp सोलर पीवी प्लांट पर भी जांच की जाती है। 96-पल्स वीएससी को विकसित करने के लिए समान पावर सर्किट कॉन्फिगरेशन वाले मॉड्यूलर 24-पल्स वीएससी के चार सेट का उपयोग किया जाता है। प्रत्येक 24-पल्स वीएससी को तीन-स्तरीय कन्वर्टर और ट्रांसफार्मर के साथ डेल्टा ओपन एलवी-वाइंडिंग्स और श्रृंखला से जुड़े विभिन्न चरण-स्थानांतरित ज़िगज़ैग एचवी-वाइंडिंग के साथ कॉन्फिगर किया गया है। सौर पीवी संयंत्र 66 केवी ग्रिड से एकीकृत है। 96-पल्स वीएससी लोअर ऑर्डर हार्मोनिक एलिमिनेशन मल्टीपल्स ट्रांसफॉर्मर (एमपीटी) कॉन्फिगरेशन के साथ महसूस किया जाता है, और चयनात्मक हार्मोनिक एलिमिनेशन (एसएचई) तकनीकों के आधार पर उपयुक्त रूप से चयनित कन्वर्टर स्विचिंग एंगल्स के साथ उच्च ऑर्डर हार्मोनिक को समाप्त कर दिया जाता है। इष्टतम सौर उत्पादन के लिए प्रत्येक पीवी स्ट्रिंग के साथ एमपीपीटी डीसी-डीसी बूस्ट कनवर्टर का उपयोग किया जाता है। ग्रिड राउंड-द-क्लॉक पावर (आरटीसी) आपूर्ति प्रदान करने के लिए एक बैटरी ऊर्जा भंडारण प्रणाली (बीईएस) पीवी उप-सरणी के साथ क्षेत्र में जुड़ी हुई है।

मल्टीलेवल कन्वर्टर पर आधारित हाई-पावर ग्रिड इंटरफेस सोलर पीवी प्लांट्स पर जांच की जाती है। फंडामेंटल फ्रीक्वेंसी स्विचिंग सेलेक्टिव हार्मोनिक एलिमिनेशन (एसएचई) मॉड्युलेटेड ग्यारह-लेवल कैस्केडेड एच-ब्रिज (सीएचबी) वीएससी का उपयोग एमएलसी अनुप्रयोगों में किया जाता है। कैपेसिटर वोल्टेज संतुलन विधि के साथ ग्यारह-स्तरीय सीएचबी वीएससी कॉन्फिगरेशन और नियंत्रण एल्गोरिदम को विस्तार से प्रस्तुत किया गया है। 20MW सौर पीवी संयंत्र बिजली में उतार-चढ़ाव और ऊर्जा समय परिवर्तन/पीक स्थानांतरण अनुप्रयोगों को कम करने के लिए उपयोग किए गए 13-स्तर सीएचबी वीएससी के आधार पर बीईएस पर भी जांच की जाती है। एक हाइब्रिड स्मूथिंग विधि प्रस्तुत की गई है, जो धूप और बादल वाले मौसम की स्थिति के लिए उपयुक्त है और बैटरी ऊर्जा के उपयोग और आकार को अनुकूलित करती है।

बैटरी स्टेट ऑफ चार्ज कंट्रोल और वीएससी एरिया इक्लाइजेशन मॉड्यूलेशन स्ट्रैटेजी (एईएमएस) को विस्तार से प्रस्तुत किया गया है।

हाई पावर ग्रिड इंटरफेस सोलर पीवी, और बीईएस सिस्टम के विभिन्न संयंत्र विन्यासों के डिजाइन, मॉडलिंग, नियंत्रण और वास्तविक समय कार्यान्वयन, जैसा कि ऊपर चर्चा की गई है, और उनके स्थिर-अवस्था, हार्मोनिक और गतिशील प्रदर्शन, स्टेटकॉम ऑपरेशन, अलग-अलग सौर विकिरण स्तरों और ग्रिड वोल्टेज में परिवर्तन के तहत मूल्यांकन किया जाता है।

3.2.2	Circuit Configuration and Operating Principle of 48-Pulse Voltage Source Converter (Configured with TLC and MWT)	30
3.3	Design of 52MWp Solar PV Plant Based on 48-Pulse VSC (Configured with TLC and MWT)	33
3.3.1	Design of Transformer	33
3.3.2	Design of PV Array	34
3.3.3	Selection of DC Link Voltage	35
3.3.4	Design of DC Link Capacitor	35
3.4	Control of 52MWp Solar PV Plant Based on 48-Pulse VSC (Configured with TLC and MWT)	35
3.5	MATLAB Modeling of 52MWp Solar PV Plant Based on 48-Pulse VSC (Configured with TLC and MWT)	40
3.6	Real-Time Implementation of 52MWp Solar PV Plant Based on 48-Pulse VSC (Configured with TLC and MWT)	42
3.7	Results and Discussion	43
3.7.1	Simulated Performance of 52MWp Solar PV Plant Based on 48-Pulse Voltage Source Converter (Configured with TLC and MWT)	43
3.7.1.1	Steady-State and Harmonics Performances	42
3.7.1.2	Dynamic Performances	46
3.7.2	Real-time Performance of 52MWp Solar PV Plant Based on 48-Pulse Voltage Source Converter (Configured with TLC and MWT)	53
3.7.2.1	Steady-State and Harmonics Performances	53
3.7.2.2	Dynamic Performances	54
3.8	Conclusions	57
CHAPTER – IV	100MWp GRID INTERFACED SOLAR PV SYSTEM BASED ON MULTI-PULSE VSC CONFIGURED WITH THREE-LEVEL NPC AND MEDIUM VOLTAGE TRANSFORMER	58-90
4.1	General	58
4.2	System Configurations for A High-Power Grid Interface Solar PV System	58
4.3	Design of Voltage Source Converters Based Solar PV Plant	63
4.3.1	Design of Transformer	63
4.3.2	Design of PV Array	64

4.3.3	Selection of DC Link Voltage	65
4.3.4	Design of DC Link Capacitor	65
4.4	Control of Voltage Source Converter Based Solar PV Plant	66
4.5	MATLAB Modeling of Voltage Source Converter Based Solar PV Plant	71
4.6	Real-Time Implementation of Voltage Source Converter Based Solar PV Plant	72
4.7	Results and Discussion	73
4.7.1	Simulated Performance of Voltage Source Converter Based Solar PV Plant	73
4.7.1.1	Steady-State and Harmonics Performances	74
4.7.1.2	Dynamic Performances	74
4.7.2	Real-time Performance of Voltage Source Converter Based Solar PV Plant	84
4.7.2.1	Steady-State and Harmonics Performances	84
4.7.2.2	Dynamic Performances	85
4.8	Conclusions	90
 CHAPTER – V		
	HIGH-POWER GRID INTERFACED SOLAR PV SYSTEM BASED ON FFS MODULATED VSC WITH DIFFERENT PHASE-SHIFTED 12-PULSE CONFIGURED TRANSFORMERS	91-113
5.1	General	91
5.2	Circuit configurations of High-Power Grid Interface Solar PV System	91
5.3	Design of Three-Level Voltage Source Converters Based Solar PV Plant	95
5.3.1	Design of Twelve Pulse Transformer	95
5.3.2	Design of PV Array	97
5.3.3	Selection of DC Link Voltage	97
5.3.4	Design of DC Link Capacitor	97
5.4	Control of Three-Level Voltage Source Converter Based Solar PV Plant	98
5.5	MATLAB Modeling of 40MWp Solar PV Plant	100
5.6	Real-Time Implementation of 40MWp Solar PV Plant	100
5.7	Results and Discussion	102
5.7.1	Simulated Performance of 40MWp Grid Interface Solar PV Plant	102
5.7.1.1	Steady-State Performances	102
5.7.1.2	Dynamic Performances	102
5.7.2	Real-time Performance of 40MWp Grid Interface Solar PV Plant	106
5.7.2.1	Steady-State and Harmonics Performances	106
5.7.2.2	Dynamic Performances	110

5.8	Conclusions	112
CHAPTER – VI	72-PULSE VSC BASED 240MWp GRID INTERFACED SOLAR PV PLANT WITH DISTRIBUTED DC-COUPLED BATTERY ENERGY STORAGE	114-150
6.1	General	114
6.2	High-Power Grid Interface Solar PV Plant Structure	114
6.3	Design of 72-Pulse VSC Based 240MWp Solar PV Plant	121
6.3.1	Design of Transformer	121
6.3.2	Design of PV Array	123
6.3.3	Selection of DC Link Voltage	123
6.3.4	Design of DC Link Capacitor	123
6.3.5	Design of BES	124
6.3.6	Design of DC-DC Converter Inductor	124
6.4	Control of 72-Pulse VSC Based 240MWp Solar PV Plant	125
6.5	MATLAB Modeling of 72-Pulse VSC Based 240MWp Solar PV Plant	130
6.6	Real-Time Implementation of 72-Pulse VSC Based 240MWp Solar PV Plant	132
6.7	Results and Discussion	133
6.7.1	Simulated Performance of 72-Pulse VSC Based 240MWp Solar PV Plant	133
6.7.1.1	Steady-State and Harmonics Performances	134
6.7.1.2	Dynamic Performances	143
6.7.2	Real-time Performance of 72-Pulse VSC Based 240MWp Solar PV Plant	146
6.7.2.1	Steady-State and Harmonics Performances	146
6.7.2.2	Dynamic Performances	147
6.8	Conclusions	150
CHAPTER – VII	225MWp SOLAR PV PLANT CONFIGURED WITH 54-PULSE VSC AND DC-COUPLED BES	151-182
7.1	General	151
7.2	High-Power Grid Interface Solar PV Plant Structure	151
7.3	Design of 54-Pulse VSC Based 225MWp Solar PV Plant	157
7.3.1	Design of Transformer	158
7.3.2	Design of PV Array	159
7.3.3	Selection of DC Link Voltage	159
7.3.4	Design of BES	159

7.3.5	Selection of DC-DC Converter Inductor	160
7.4	Control of 54-Pulse VSC Based 225MWp Solar PV Plant	160
7.5	MATLAB Modeling of 225MWp Solar PV Plant	163
7.6	Real-Time Implementation 225MWp Solar PV Plant	165
7.7	Results and Discussion	165
7.7.1	Simulated Performance of 54-Pulse VSC Based 225MWp Solar PV Plant	165
7.7.1.1	Steady-State and Harmonics Performances	165
7.7.1.2	Dynamic Performances	173
7.7.2	Real-time Performance of 54-Pulse VSC Based 225MWp Solar PV Plant	176
7.7.2.1	Steady-State and Harmonics Performances	176
7.7.2.2	Dynamic Performances	177
7.8	Conclusions	181
 CHAPTER – VIII GRID INTERFACED 480MWp SOLAR PV PLANT BASED ON MODULAR 96-PULSE VSC AND BATTERY ENERGY STORAGE		183-215
8.1	General	183
8.2	Structure of Solar PV Plant of 480MWp Capacity	183
8.3	Design of Solar PV Plant of 480MWp Capacity	191
8.3.1	Design of Transformer	191
8.3.2	Design of PV Array	192
8.3.3	Selection of DC Link Voltage	193
8.3.4	Design of DC Link Capacitor	193
8.3.5	Design of BES	194
8.3.6	Design of DC-DC Converter Inductor	194
8.4	Control of Solar PV Plant of 480MWp Capacity	195
8.5	MATLAB Modeling of Solar PV Plant of 480MWp Capacity	198
8.6	Real-Time Implementation of Solar PV Plant of 480MWp Capacity	198
8.7	Results and Discussion	201
8.7.1	Simulated Performance of Solar PV Plant of 480MWp Capacity	202
8.7.1.1	Steady-State and Harmonics Performances	202
8.7.1.2	Dynamic Performances	207
8.7.2	Real-time Performance of Solar PV Plant of 480MWp Capacity	212
8.7.2.1	Steady-State and Harmonics Performances	212

	8.7.2.2	Dynamic Performances	213
8.8		Conclusions	215
CHAPTER – IX		HIGH POWER GRID INTERFACED SOLAR PV SYSTEM BASED ON MULTILEVEL CONVERTER	216-240
9.1		General	216
9.2		Circuit Configuration of High Power Grid Interfaced Solar PV System	216
9.3		Design High Power Grid Interfaced Solar PV System	218
	9.3.1	Design of Transformer	219
	9.3.2	Design of PV Array	220
	9.3.3	Selection of H-bridge DC Link Voltage	221
	9.3.4	Design of H-Bridge DC Link Capacitor	221
	9.3.6	Operating Principle of Eleven-Level CHB MLC	221
9.4		Control of MLC Based 40MWp Grid Interfaced Solar PV System	223
9.5		MATLAB Modeling	228
9.6		Real-Time Implementation	228
9.7		Results and Discussion	230
	9.7.1	Simulated Performance of Eleven-Level MLC Based 40MWp Solar PV Plant	230
		9.7.1.1 Steady-State and Harmonics Performances	230
		9.7.1.2 Dynamic Performances	233
	9.7.2	Real-time Performance of Eleven-Level MLC Based 40MWp Solar PV Plant	236
		9.7.2.1 Steady-State and Harmonics Performances	236
		9.7.2.2 Dynamic Performances	238
9.8		Conclusions	240
CHAPTER – X		BATTERY ENERGY STORAGE SYSTEM BASED ON MULTILEVEL CONVERTER USED IN HIGH POWER GRID INTERFACED SOLAR PV SYSTEM	241-273
10.1		General	241
10.2		Circuit Configurations of Battery Energy Storage (BES) System for High Power Grid Interfaced Solar PV System	241
10.3		Design of Battery Energy Storage System	243
	10.3.1	Design of Transformer	243
	10.3.2	Design of Battery Array	246
	10.3.3	Selection of H-bridge DC Link Voltage	246

10.3.5	Operating Principle of 13-Level CHB MLC	247
10.4	Control of BES System	251
10.4.1	BES Control Algorithm for Solar PV Generation Smoothing	251
10.4.2	BES Control Algorithm for Solar PV Generation Energy-Time Shifting/Peak-Shaving	254
10.4.3	BES State-of-Charge (SOC) Computation	254
10.4.4	Control of Thirteen-Level CHB MLC	255
10.5	MATLAB Modeling	258
10.6	Real-Time Implementation	258
10.7	Results and Discussion	259
10.7.1	Simulated Performance of Thirteen-Level MLC Based BES	259
10.7.1.1	Steady-State and Harmonics Performances	260
10.7.1.2	Dynamic Performances	263
10.7.2	Real-time Performance of Thirteen-Level MLC Based BES	263
10.7.2.1	Steady-State and Harmonics Performances	263
10.7.2.2	Dynamic Performances	267
10.8	Conclusions	273
CHAPTER – XI	MAIN CONCLUSIONS AND SUGGESTIONS FOR FURTHER WORK	274-282
11.1	General	274
11.2	Main Conclusions	275
11.3	Suggestion for Future Work	281
	APPENDICES	283
	REFERENCES	285
	LIST OF PUBLICATIONS	299
	BOI-DATA	301

LIST OF FIGURES

- Fig. 3.1 System configuration for 52MWp solar PV plant.
- Fig. 3.2 A 48-pulse VSC with TLC and MWT for 52MW solar PV plant: (a) circuit configuration, (b) schematic of a string combiner box and (c) voltage control mode.
- Fig. 3.3 Two-level VSC: (a) circuit configuration, and (b) line voltage waveform.
- Fig. 3.4 Star-delta and delta-delta transformer configuration.
- Fig. 3.5 Control algorithm of a 48-pulse VSC.
- Fig. 3.6 INC-based MPPT algorithm: (a) INC-based MPPT approach, (b) Flow-diagram of INC-MPPT Algorithm.
- Fig. 3.7 52MWp solar PV plant MATLAB model.
- Fig. 3.8 Real-time implementation: (a) real-time execution block diagram, and (b) Laboratory real-time setup.
- Fig. 3.9 Simulated steady-state 48-pulse VSC (configured with TLC and MWT): (a) voltage waveform, and (b) harmonics profile.
- Fig. 3.10 Simulated solar PV plant grid current: (a) steady-state waveform and (b) harmonics profile.
- Fig. 3.11 Simulated dynamic response of solar PV plant based on 48-pulse VSC (configured with TLC and MWT) with decrease in solar irradiance.
- Fig. 3.12 Simulated dynamic response of solar PV plant based on 48-pulse VSC (configured with TLC and MWT) with a decrease in solar irradiance (with 15% transformer impedance).
- Fig. 3.13 Fig.3.12. Simulated capacitive reactive power dynamic response of solar PV plant based on 48-pulse VSC (configured with TLC and MWT).
- Fig. 3.14 Simulated inductive reactive power dynamic response of solar PV plant based on 48-pulse VSC (configured with TLC and MWT).
- Fig. 3.15 Simulated inductive reactive power dynamic response of solar PV plant based on 48-pulse VSC (configured with TLC and MWT) with 15% transformer impedance.
- Fig. 3.16 Real-time steady-state 48-pulse VSC (configured with TLC and MWT) line voltage waveform.
- Fig. 3.17 Real-time steady-state grid current waveform of 52MWp solar PV plant based on 48-pulse VSC (configured with TLC and MWT).
- Fig. 3.18 Real-time dynamic response of 48-pulse VSC (configured with TLC and MWT) based 52MWp solar PV plant with increase in solar irradiance.
- Fig. 3.19 Real-time capacitive reactive power dynamic response of 48-pulse VSC (configured with TLC and MWT) based 52MWp solar PV plant.
- Fig. 3.20 Real-time inductive reactive power dynamic response of 48-pulse VSC (configured with TLC and MWT) based 52MWp solar PV plant.

- Fig. 4.1 High power solar PV plant configuration.
- Fig.4.2 A 48-pulse VSC configured for 100MWp solar PV plant : (a) circuit configuration, (b) NPCs grouping, and (c) voltage control mode.
- Fig.4.3 An NPC: (a) circuit configuration, and (b) waveform for phase and line voltage.
- Fig.4.4 Transformer configuration.
- Fig. 4.5 VSC control strategy.
- Fig.4.6 Q-V droop control strategy.
- Fig. 4.7 MATLAB model of a 100MWp solar PV plant based on 48-pulse VSC.
- Fig. 4.8 Simulated steady-state 48-pulse VSC: (a) voltage waveform and (b) harmonics profile.
- Fig. 4.9 Simulated 100MWp solar PV plant grid current: (a) steady-state waveform and (b) harmonics profile.
- Fig. 4.10 Simulated dynamic performance of 48-pulse VSC based 100MWp solar PV plant with change in solar irradiance from 1000W/m² to 600W/m².
- Fig. 4.11 Simulated dynamic performance of 48-pulse VSC based 100MWp solar PV plant with change in solar irradiance from 600W/m² to 1000W/m².
- Fig. 4.12 Simulated daytime reactive power dynamic performance of 48-pulse VSC based 100MWp solar PV plant with change in grid voltage from 1.0 pu to 0.9 pu.
- Fig.4.13 Simulated nighttime reactive power dynamic performance of 48-pulse VSC based 100MWp solar PV plant with change in grid voltage from 1.0 pu to 1.1 pu.
- Fig.4.14 Simulated nighttime reactive power dynamic performance of 48-pulse VSC based 100MWp solar PV plant with change in grid voltage from 1.0 pu to 0.9 pu.
- Fig.4.15 Simulated nighttime reactive power dynamic performance of 48-pulse VSC based 100MWp solar PV plant with change in grid voltage from 1.0 pu to 1.1 pu.
- Fig.4.16 Real-time steady-state 48-pulse VSC line voltage waveform.
- Fig.4.17 Real-time steady-state solar PV plant grid current waveform.
- Fig.4.18 Real-time dynamic response of solar PV plant with change in solar irradiance from 1000 to 600 W/m².
- Fig.4.19 Real-time dynamic response of solar PV plant with change in solar irradiance from 600 to 1000 W/m².
- Fig.4.20 Real-time daytime reactive power dynamic response of solar PV plant with change in grid voltage from 1.0 pu to 0.9 pu.

- Fig.4.21 Real-time daytime reactive power dynamic response of solar PV plant with change in grid voltage from 1.0 pu to 1.1 pu.
- Fig.4.22 Real-time nighttime reactive power dynamic response of solar PV plant with change in grid voltage from 1.0 pu to 0.9 pu.
- Fig.4.23 Real-time nighttime reactive power dynamic response of solar PV plant with change in grid voltage from 1.0 pu to 1.1 pu.
- Fig. 5.1 System configuration for 40MWp solar PV power generating system.
- Fig.5.2 Three-level-NPC VSC configuration, output ac voltage waveforms, and pulse generation: (a) NCP VSC configuration, (b) phase to dc neutral voltage and switching pulse generation, and (c) line voltage waveform.
- Fig.5.3 Delta/ zigzag configured transformer for positive and phase negative phase shifting.
- Fig.5.4 Control algorithm for NCP-VSC.
- Fig. 5.5 MATLAB modeling for 40MWp solar PV plant.
- Fig.5.6 Simulated steady-state VSC: (a) Voltage waveform and (b) harmonics profile.
- Fig. 5.7 Simulated steady-state waveform with solar irradiance 1000W/m^2
- Fig. 5.8 Simulated solar PV plant dynamic response with change in solar irradiance from 1000W/m^2 to 600W/m^2 .
- Fig. 5.9 Simulated solar PV plant dynamic response with change in solar irradiance from 600W/m^2 to 1000W/m^2 .
- Fig. 5.10. Steady-state VSC line voltage and current waveform and their harmonics profiles: (a) Voltage waveform and it is harmonics profile, (b) Current waveform and it is harmonics profile.
- Fig. 5.11 Steady-state current and harmonics profiles: Transformer HV side.
- Fig. 5.12 Steady-state current and harmonics profiles: local-pooling switchgear output.
- Fig.5.13 Steady-state current and harmonics profiles: grid connection point (at PCC).
- Fig.5.14 Solar PV plant dynamic response with change in solar irradiance from 1000W/m^2 to 600W/m^2 .
- Fig. 5.15 Solar PV plant dynamic response with change in solar irradiance from 600W/m^2 to 1000W/m^2 .
- Fig. 6.1 Circuit architecture of a 240MWp solar PV-BES plant.
- Fig.6.2 Solar PV-BES plant generation curve
- Fig. 6.3 Configuration of a 72-pulse VSC
- Fig.6.4 Phasor diagram for determining the effective switching angle for 72-pulse VSC operation
- Fig. 6.5 NPC phase voltage

- Fig. 6.6 A NPC set circuit configuration
- Fig. 6.7 Transformer windings connection, (a) positive phase-shift and (b) negative phase-shift.
- Fig. 6.8 72-pulse VSC control strategy.
- Fig. 6.9 MATLAB model of a 240MWp solar PV plant.
- Fig. 6.10 Real-time implementation: (a) execution block diagram, (b) laboratory setup.
- Fig. 6.11 72-pulse VSC line voltage waveform and harmonics at 110% of nominal output voltage.
- Fig. 6.12 72-pulse VSC line voltage waveform and harmonics at 100% of nominal output voltage.
- Fig. 6.13 72-pulse VSC line voltage waveform and harmonics at 90% of nominal output voltage
- Fig. 6.14 Simulated solar PV plant grid current: (a) steady-state waveform and (b) harmonics profile.
- Fig. 6.15 72-pulse VSC steady-state waveform with rated active power generation.
- Fig. 6.16 72-pulse VSC steady-state waveform with rated reactive power generation.
- Fig. 6.17 72-pulse VSC steady-state operation with different solar irradiance (multi-MPPT operation).
- Fig. 6.18 Response of solar PV-BES plant with decrease in solar radiation.
- Fig. 6.19 Response of solar PV-BES plant with continuous change in solar radiation.
- Fig. 6.20 Solar PV-BES plant real-time steady-state response
- Fig. 6.21 72-pulse VSC real-time steady-state line voltage waveform.
- Fig. 6.22 Solar PV-BES plant real-time steady-state grid current waveform.
- Fig. 6.23 Solar PV-BES plant real-time dynamic response change in active power.
- Fig. 6.24 Solar PV-BES plant real-time inductive capacitive power dynamic response.
- Fig. 6.25 Solar PV-BES plant real-time inductive reactive power dynamic response.
- Fig. 7.1 Circuit configuration for 225MWp solar PV-BES power generating system.
- Fig.7.2 Field side DC connection: (a) PV array and DC-DC converter connection, and (b) boost converter circuit configuration.
- Fig. 7.3 A 54-pulse VSC with PV and BES circuit configuration.
- Fig.7.4 VSC voltage control method
- Fig. 7.5 Circuit of the TLC converter and phase voltage waveform
- Fig. 7.6 Zigzag-delta transformer winding configuration, (a) '+ve phase shifting and (b) '-ve phase shifting
- Fig. 7.7 Control strategy for solar PV plant with BES
- Fig. 7.8 MATLAB model of a 225MWp solar PV plant

- Fig. 7.9 Simulated steady-state: (a) voltage-waveform and (b) voltage-harmonics profile of 18-pulse VSC.
- Fig. 7.10 Simulated steady-state voltage waveform of 18-pulse VSCs and 54-pulse VSC.
- Fig.7.11 Simulated 54-pulse VSC line voltage: (a) steady-state waveform and (b) harmonics profile under 110% of nominal voltage.
- Fig.7.12 Simulated 54-pulse VSC line voltage: (a) steady-state waveform and (b) harmonics profile under 100% of nominal voltage.
- Fig.7.13 Simulated 54-pulse VSC line voltage: (a) steady-state waveform and (b) harmonics profile under 90% of nominal voltage.
- Fig.7.14 Simulated 54-pulse VSC based solar PV plant grid current: (a) steady-state waveform and (b) harmonics profile.
- Fig.7.15 Solar PV-BES plant simulated response to the increase in solar radiation.
- Fig.7.16 Solar PV-BES plant simulated response to the decrease in solar radiation.
- Fig.7.17 Solar PV-BES plant steady-state waveform obtained in real-time
- Fig.7.18 A 54-pulse VSC line voltage waveform and its power quality performance obtained in real-time.
- Fig.7.19 Grid current waveform and its power quality performance are obtained in real-time.
- Fig.7.20 Real-time solar PV and BES plant response under an increase in solar radiation.
- Fig.7.21 Real-time solar PV and BES plant response under a decrease in solar radiation.
- Fig.7.22 Real-time solar PV and BES plant response under an increase in active power.
- Fig.7.23 Real-time solar PV and BES plant response under a decrease in grid voltage.
- Fig.7.24 Real-time solar PV and BES plant response under an increase in grid voltage.
- Fig. 8.1 480MWp solar PV-BES plant configuration
- Fig.8.2 A 96-pulse VSC circuit configuration
- Fig. 8.3 Group-A and B NPCs phase voltage
- Fig.8.4 VSC NPC and SCB connection
- Fig.8.5 Windings configuration of VSC medium voltage transformer, (a) primary winding with positive phase-shift and (b) primary winding with negative phase-shift.
- Fig.8.6 Control block diagram for 96-pulse VSC
- Fig.8.7 MATLAB-Simulink model of a solar PV plant of 480MWp capacity
- Fig. 8.8 OPAL-RT deployment: (a) execution flowchart, and (b) setup.

- Fig. 8.9 24-pulse VSC voltage realization: (a) steady-state voltage-waveform and (b) 24-pulse VSC harmonics profile.
- Fig. 8.10 Steady-state voltage waveform of 24-pulse VSCs and 96-pulse VSC.
- Fig. 8.11 Line voltage waveform of a 96-pulse VSC and its harmonics spectrum.
- Fig.8.12 Grid current waveform of solar PV plant and its harmonics spectrum.
- Fig. 8.13 Response under an increase in solar irradiance.
- Fig.8.14 Response under with increase in grid power during non-solar hours.
- Fig.8.15 Capacitive reactive power response.
- Fig.8.16 Inductive reactive power response.
- Fig.8.17 Real-time steady-state line voltage waveform of a 96-pulse VSC.
- Fig. 8.18 Real-time steady-state solar PV plant grid current waveform.
- Fig.8.19 Real-time dynamic response of solar PV plant with change in solar irradiance.
- Fig.8.20 Real-time dynamic response of solar PV plant with change in reactive power.
- Fig. 9.1 System configuration for 40MWp solar PV power generating system.
- Fig.9.2 Eleven-level CHB VSC configuration and output voltage waveforms: (a) VSC configuration and (b) phase voltage waveform.
- Fig.9.3 Star/Delta-Delta configured transformer.
- Fig.9.4 VSC control algorithms: (a) DQ-based control algorithm, and (b) DC capacitors voltage balancing methods.
- Fig.9.5 MATLAB model of a 40MWp solar PV plant.
- Fig.9.6 Simulated steady-state VSC: (a) voltage waveform, and (b) harmonics profile.
- Fig. 9.7. Simulated solar PV plant steady-state current: (a) waveform and (b) harmonics profile.
- Fig. 9.8 Dynamic response: VSC under the change in solar irradiance condition.
- Fig. 9.9 Dynamic response: VSC under the change in temperature condition.
- Fig.9.10 Real-time steady-state waveform with solar irradiance $1000\text{W}/\text{m}^2$.
- Fig. 9.11 Real-time steady-state VSC line voltage waveform and its harmonics spectrum.
- Fig. 9.12 Real-time steady-state grid current waveform and harmonics spectrum.
- Fig.9.13 Solar PV plant dynamic response in real-time with change in solar irradiance from $1000\text{W}/\text{m}^2$ to $600\text{W}/\text{m}^2$
- Fig.9.14 Solar PV plant dynamic response in real-time with change in solar irradiance from $600\text{W}/\text{m}^2$ to $1000\text{W}/\text{m}^2$
- Fig.10.1 System configuration for solar PV and BES

- Fig.10.2 Circuit configuration and waveform: (a) 13-level CHB VSC configuration, and (b) voltage waveform phase-DC neutral.
- Fig.10.3 Star/Delta-Delta configured transformer.
- Fig.10.4 Area equalizations modulation strategy.
- Fig.10.5 BES smoothening algorithm
- Fig.10.6 BES Energy-Time Shifting/Peak-Shaving algorithm
- Fig.10.7 VSC control algorithms
- Fig.10.8 MATLAB model of solar PV with BES plant
- Fig.10.9 Simulated steady-state 13-level VSC: (a) voltage waveform and (b) harmonics profile
- Fig.10.10 Simulated steady-state BES plant current: (a) waveform and (b) harmonics profile
- Fig.10.11 Simulated 13-level VSC dynamic response with battery in charging mode
- Fig.10.12 Simulated 13-level VSC dynamic response with battery in discharging mode
- Fig.10.13 Steady-state BES real-time voltage and current waveform
- Fig.10.14 Steady-state real-time BES VSC voltage waveform and harmonics profile
- Fig.10.15 Steady-state real-time BES plant output current waveform and harmonics profile
- Fig.10.16 BES real-time dynamic response with change in solar irradiance from 1000 W/m² to 600 W/m².
- Fig.10.17 BES real-time dynamic response with change in solar irradiance from 600W/m² to 1000W/m²
- Fig.10.18 Real-time dynamic performance with continuous change in solar irradiance with the step of 200W/m²
- Fig.10.19 Historical solar irradiance profile
- Fig.10.20 Real-time dynamic performance with continuous change in solar irradiance
- Fig.10.21 Real-time dynamic performance with continuous change in solar irradiance: SOC of battery array connected with individual H-bridge of CHB VSC.

LIST OF TABLES

Table 3.1	TLCs Switching Phase Displacement Angles.
Table 3.2	48-Pulse VSC based Solar PV Plant Current THD with Different Solar Irradiance.
Table 3.3	48-Pulse VSC based Solar PV Plant Current THD with Different Solar Irradiance (Transformer Impedance 15.0%)
Table 4.1	Selection Of Optimum VSC Dead Angle.
Table 6.1	Grid Current THD of a 100MWp Solar PV Plant Under Different Solar Irradiance.
Table 6.2	Zigzag Windings Phase-Shift Angles and NPC's Switching Angles.
Table 6.3	NPC's Effective Switching Angles for 72-Pulse VSC Operation.
Table 6.4	Table 6.3 Calculation of a_1 and a_2
Table 6.5	240MWp Solar PV Plant Grid Current THD Under Different Plant Generation.
Table 7.1	54-Pulse VSC based Solar PV Plant Current THD with Different Generation.
Table 8.1	NPC's Switching Angles and Switching Sequence
Table 8.2	Calculation of w_1 and w_2
Table 8.3	Solar PV Plant Grid Current THD
Table 9.1	H-Bridge Switching States and Their Representation
Table 9.2	Switching Angles (Degree) for Different M
Table 9.3	Switching Patterns of 11-Level CHB VSC
Table 9.4	Switching sequence for different values of M ($X=R, Y, B$) of 11-Level CHB VSC
Table 9.5	Solar PV Plant Current THD with Output Power
Table 10.1	13-level VSC H-Bridge Switching States and Their Representation
Table 10.2	Switching Patterns of a 13-level VSC
Table 10.3	Switching Sequence for Different Values of M ($X=R, Y, B$) of 13-level VSC
Table 10.4	BES Plant Current THD

LIST OF ABBREVIATIONS

AC	Alternating Current
AEMS	Area Equalizations Modulation Strategy
BES	Battery Energy Storage
BOS	Balance Of System
CHB	Cascaded H-Bridge
DC	Direct Current
DPC	Direct Power Control
DQ	Decoupled
FACTS	Flexible Alternating Current Transmission Systems
FFS	Fundamental Frequency Switching
HVDC	High Voltage DC
IGBTs	Insulated Gate Bipolar Transistors
ILST	Improved Linear Sinusoidal Tracer
INC	Incremental Conductance
IPT	Instantaneous Reactive Power Theory
LCC	Life Cycle Cost
LIBS	Lithium-ion battery systems
LPF	Low Pass Filter
LV	Low Voltage
MLC	Multi-Level Converter
MPP	Maximum Power Point
MPPT	Maximum Power Point Tracking
MPT	Multipulse Transformer
MV	Medium Voltage
MWT	Multi-Windings Transformer
NPC	Neutral Point Clamp
PCC	Point of Common Coupling
PCU	Power Conditioning Unit
PCS	Power Conditioning System
P&O	Perturb and Observe
PST	Phase-Shifting Transformers
PI	Proportional Integral
PLL	Phase Locked Loop

PV	Photo Voltaic
PWM	Pulse Width Modulation
RE	Renewable Energy
RR	Ramp Rate
RT	Real Time
SCB	String Combiner Box
SHE	Selective Harmonic Elimination
SMA	Simple Moving Average
SOC	State Of Charge
SPWM	Sinusoidal Pulse Width Modulation
STATCOM	Static Compensator
SVM	Space-Vector Modulation
THD	Total Harmonic Distortion
VSC	Voltage Source Converter

LIST OF SYMBOLS

V_{ab}, V_{bc}, V_{ca}	Line voltages
V_a, V_b, V_c	Phase voltages
i_a, i_b, i_c	Line current
V_r, V_y, V_b	Phase voltages
i_r, i_y, i_b	Line current
V_d, V_q	Voltage direct and quadrature axis component
i_d, i_q	Current direct and quadrature axis component
V_α, V_β	$\alpha\beta$ -axis voltage component
i_α, i_β	$\alpha\beta$ -axis current component
V_m	Voltage magnitude
V_{LL}	Line voltage
V_{min}	Minimum voltage
V_{max}	Maximum voltage
Q_{min}	Minimum reactive power
Q_{max}	Maximum reactive power
δ	Load angle
σ	Conduction angle
β	Dead angle
V_f	Fundamental line voltage amplitude
m	Transformer turn-ratio
m_1	Transformer turn-ratio
m_2	Transformer turn-ratio
N_{series}	Number of PV modules connected in series
$N_{parallel}$	Number of PV string connected in parallel
N_s	Number of PV modules connected in series
N_p	Number of PV string connected in parallel
V_{oc}	PV module open circuit voltage
V_{mp}	PV module voltage at maximum power point
W_p	PV module power
V_{dc}	VSC DC link voltage
M	Modulation index
V_{mp}	Voltage of one module at maximum power point

I_{mp}	Current of one module at maximum power point
P_{dc}	DC power
P_{pv}	PV array power
V_{pv}	PV array voltage
I_{pv}	PV array current
L_B	Inductor inductance
ΔI_{in}	Current ripple
f_{sw}	Switching frequency of VSC
V_{dcref}	Reference DC bus voltage
C_{dc}	DC link capacitor voltage
K_{pd} and K_{id}	Proportional and integral constant of DC link voltage controller
P, Q	Active and reactive power
A_r	Reference signal amplitude
A_c	Carrier signal amplitude
P_{bm}	Battery module power rating
E_{bm}	Battery module energy rating
N_{sb}	Number of battery module connected in series
N_{pb}	Number of battery module connected in parallel
D	Duty ratio